



**HAL**  
open science

## Oily bioorganoclays in drilling fluids: Micro and macroscopic properties

Qiang Li, Laurence de Viguerie, Lucie Laporte, Romain Berraud-Pache,  
Guangzheng Zhuang, Christelle Souprayen, Maguy Jaber

► **To cite this version:**

Qiang Li, Laurence de Viguerie, Lucie Laporte, Romain Berraud-Pache, Guangzheng Zhuang, et al.. Oily bioorganoclays in drilling fluids: Micro and macroscopic properties. Applied Clay Science, 2024, 247, pp.107186. 10.1016/j.clay.2023.107186 . hal-04443274

**HAL Id: hal-04443274**

**<https://hal.science/hal-04443274>**

Submitted on 7 Feb 2024

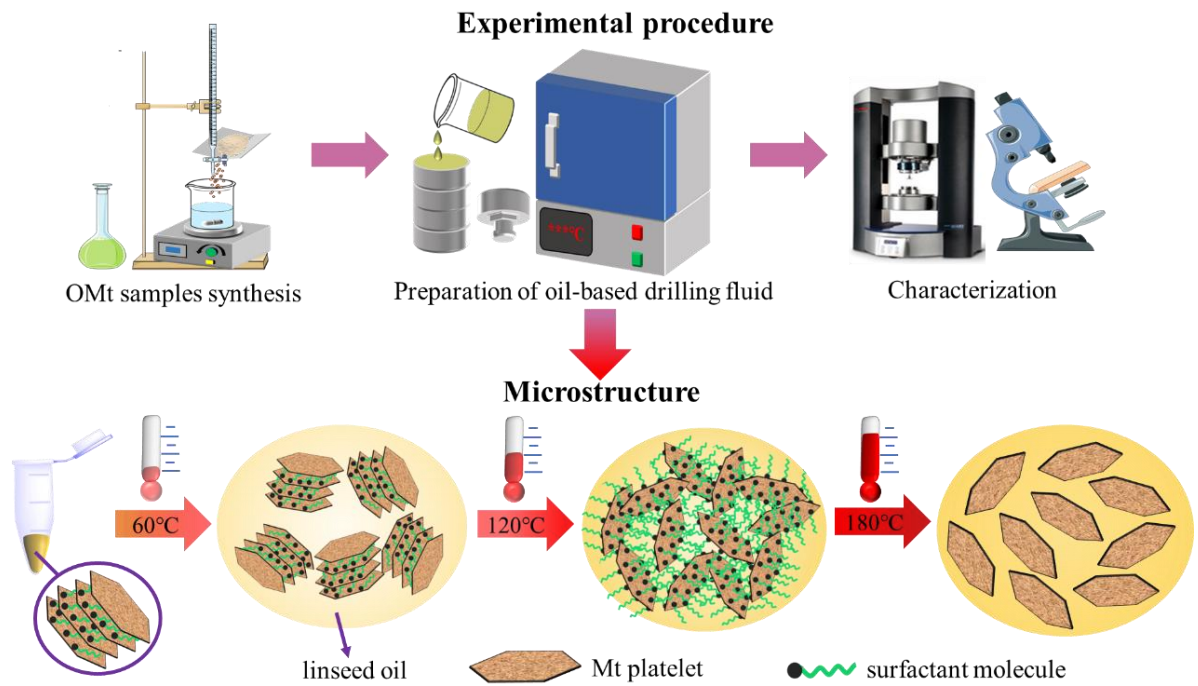
**HAL** is a multi-disciplinary open access archive for the deposit and dissemination of scientific research documents, whether they are published or not. The documents may come from teaching and research institutions in France or abroad, or from public or private research centers.

L'archive ouverte pluridisciplinaire **HAL**, est destinée au dépôt et à la diffusion de documents scientifiques de niveau recherche, publiés ou non, émanant des établissements d'enseignement et de recherche français ou étrangers, des laboratoires publics ou privés.



23 engineering.

24 **Graphical abstract**



25

26 **Keywords:** oil-based drilling fluids; organoclay; vegetable oil; microstructure;

27 rheology; viscoelasticity

28

29

30

31

32

33

34

35

36

37

38

### 39 *1. Introduction*

40 The depletion of easily accessible hydrocarbon resources has prompted the  
41 petroleum industry to develop more complex and challenging reservoirs, such as  
42 unconventional shales and high-temperature and high-pressure (HTHP) fields. Shale  
43 reservoirs are rich in clay minerals, and various reactions will occur when exposed to  
44 water-based drilling fluids, which may cause wellbore instability (Deville et al., 2011;  
45 Aramendiz and Imqam, 2019). Drilling in HTHP conditions is a challenging task as  
46 the harsh environments adversely affect drilling fluid performance (Zhong et al.,  
47 2023). Consequently, the selection of the appropriate drilling fluids plays a pivotal  
48 role in trouble-free and safe drilling operations. Oil-based drilling fluids have high  
49 thermal stability and can provide low friction, shale inhibition, and salt resistance to  
50 overcome some undesirable characteristics of water-based drilling fluids (Zhuang et  
51 al., 2019). Therefore, oil-based drilling fluids are more suitable for shale and HTHP  
52 drilling.

53 The ideal oil-based drilling fluid is a non-Newtonian fluid with appropriate  
54 rheological and viscoelastic properties. Organoclays are the most important additives  
55 used to adjust the colloidal and rheological properties of oil-based drilling fluids. The  
56 organoclays is known for its ability to swell and form thixotropic gels in organic  
57 media (Moraru, 2001). Most oil-based drilling fluids are formulated with clays  
58 modified with quaternary ammonium salts, although these salts are toxic and difficult  
59 to degrade. Bio-organoclays are considered to have the potential to replace traditional

60 toxic organoclays. These bio-organoclays can be obtained by modifying clay minerals  
61 with biosurfactants. Phospholipids, especially lecithin, have been investigated as  
62 promising candidates for the synthesis of bio-organoclays owing to their exceptional  
63 zwitterionic properties (Li et al., 2023b). Lecithin is usually extracted from soybeans  
64 and is mainly composed of phosphatidylcholine (PC). PC contains a choline part  
65 characterized by a negatively charged phosphate group and a positively charged  
66 trimethyl-amino group. It can prepare organic montmorillonite through ion-dipole  
67 interactions under alkaline conditions (Li et al., 2023a).

68       The rheology of oil-based drilling fluids is not only influenced by the properties  
69 and concentration of organoclays, but also affected by the composition and nature of  
70 base oil (Hermoso et al., 2014). Diesel and mineral oil are common organic dispersion  
71 mediums for preparing oil-based drilling fluids, but these materials will cause serious  
72 pollution. The drilling cuttings contaminated with oil-based drilling fluids, drilling  
73 fluid wastes and other potential contaminants pose several risks to the terrestrial,  
74 aquatic and aerial environments if not disposed of properly (Pereira et al., 2022). To  
75 address this problem, some eco-friendly, cheap and easily available vegetable oil such  
76 as palm oil (Sulaimon et al., 2017) and soybean oil (Agwu et al., 2015) have been  
77 gradually utilized as dispersion mediums in recent years.

78       The main components of most vegetable oils are triglycerides and fatty acids.  
79 Some vegetable oils, referred to as siccative oils (such as linseed oil), contain  
80 unsaturated fatty esters which can undergo a complex autoxidation mechanism  
81 followed by crosslinking, resulting in the formation of a polymer network (Orlova et

82 al., 2021). This network structure has the ability to cure and form a solid film. The  
83 curing process can be accelerated by heating or adding metallic driers (i.e.  $\text{Pb}^{2+}$ ,  $\text{Zn}^{2+}$ ),  
84 which is a common practice in oil paints (de Viguerie et al., 2016; Artesani, 2020).  
85  $\text{Zn}^{2+}$  in the siccative oil leads to the formation of carboxylic salts that behave as ionic  
86 cross-links and act as a reinforcing site for the ionomer network (Artesani, 2020). The  
87 metallic driers and siccative oils are commonly employed in oil paints, but are rarely  
88 reported in the field of oil-based drilling fluids. Additionally, temperature can have an  
89 adverse impact on the performance of organoclays in oil-based drilling fluids.  
90 Although previous studies have evaluated the macro-rheological properties of  
91 oil-based drilling fluids at high temperatures (Patel et al., 2019b; de Brito Buriti et al.,  
92 2022), the response of organoclay microstructure in oil to temperature still deserves  
93 further investigation.

94 In this study, inspired by the zinc cations and siccative oil in oil paints, the  
95 biosurfactant lecithin was used to modify Mt containing  $\text{Zn}^{2+}$  to prepare organoclays,  
96 which were then mixed with linseed oil to produce oil-based drilling fluid colloidal  
97 systems. The microstructure of ZnOMt in mineral oil (paraffin oil) and vegetable oil  
98 (linseed oil) and its effect on the rheological behavior of oil-based drilling fluids were  
99 comparatively evaluated. The X-ray diffraction (XRD) and transmission electron  
100 microscopy (TEM) techniques were employed to study the microstructure of ZnOMt  
101 suspensions.

## 102 ***2. Materials and methods***

### 103 ***2.1 Materials***

104 The chemicals used for the synthesis of the Mt are hydrofluoric acid (40% w/w;  
 105 Fluka), sodium acetate (99%; Sigma-Aldrich), magnesium acetate tetrahydrate (99%;  
 106 Sigma-Aldrich), aluminium oxide (99%; Sigma-Aldrich) and silica (99.8%; DEGU).  
 107 The materials used to prepare ZnOMt include: zinc acetate dihydrate (98%;  
 108 Sigma-Aldrich), lecithin (94%; Sigma-Aldrich), CH<sub>3</sub>CH<sub>2</sub>OH (96%; Sigma-Aldrich),  
 109 NaOH (1 mol/L; Sigma-Aldrich). The base oil utilized for formulating oil-based  
 110 drilling fluid is categorized into two types: paraffin oil and linseed oil, both procured  
 111 from Sigma-Aldrich. Their physical and chemical properties are shown in Table 1. All  
 112 chemicals were used directly without additional purification.

113 Table 1 Physical and chemical properties of paraffin oil and linseed oil

	freezing point	boiling point	flash point	density	viscosity (Pa·s, 25°C)	color	main components
linseed oil	< -24 °C	>316 °C	>113 °C	0.93 g/ml at 25 °C	0.05	yellow	triglycerides
paraffin oil	< -15 °C	260~450 °C	>215 °C	0.83~0.89 g/ml at 20 °C	0.13	colorless	higher alkanes

## 114 2.2 Synthesis of Mt

115 The Mt employed in this work was synthesized according to the previous method  
 116 (Jaber and Miéché-Brendlé, 2005; de Oliveira et al., 2021) and had the ideal formula  
 117 per half unit cell: Na<sub>0.4</sub>[Si<sub>4</sub>Al<sub>1.6</sub>Mg<sub>0.4</sub>O<sub>10</sub>(OH, F)<sub>2</sub>]. The solution is obtained by adding  
 118 the reagents in the following order: deionized water (65.61g: 3.65mol), hydrofluoric  
 119 acid (0.81g: 2.02mmol), sodium acetate (0.32g: 3.90mmol), magnesium acetate  
 120 tetrahydrate (0.86g: 4.01mmol), aluminium oxide (1.11g: 10.89mmol) and silica  
 121 (2.42g: 0.04mol). The initial hydrogel was continuously stirred at 25°C for 4.0h and  
 122 then transferred to an autoclave and heated at 190°C for 7days. The autoclave was

123 cooled to room temperature and the product was thoroughly washed with distilled  
124 water and centrifuged. Finally, the synthesized Mt was dried at 60°C for 48h. The  
125 cation exchange capacity (CEC) of the synthesized Mt is 130meq/100g.

### 126 ***2.3 Synthesis of ZnOMt***

127 The Mt structure are negatively charged due to isomorphic substitution, resulting  
128 in the presence of exchangeable hydrated cations in the interlayer space to neutralize  
129 the negative charges (Malamis and Katsou, 2013). This property of Mt makes it easy  
130 to exchange interlayer cations with other metal cations in solution to prepare Mt  
131 containing different interlayer cations. This practice has been reported in numerous  
132 literatures (Yan and Zhang, 2021). To ensure that Na<sup>+</sup> in the Mt is completely replaced  
133 by Zn<sup>2+</sup>, Mt was dispersed in 5.0CEC of zinc acetate solutions for 12h under magnetic  
134 stirring at 25°C. Then, the obtained mixture solution was centrifuged, and the same  
135 process was repeated twice. Finally, the sample was dried in an oven at 60°C for 48h.  
136 The sample will be designated as ZnMt.

137 The preparation of ZnOMt was performed using the following procedure: 2g of  
138 ZnMt was dispersed in 100mL of distilled water and stirred for 2h. 1.0CEC of lecithin  
139 was dissolved in 100mL ethanol and stirred for 2h. Next, the lecithin solution was  
140 slowly added to the ZnMt dispersion and then NaOH was added dropwise to confirm  
141 that the pH of the mixture solution was 9.0. The mixture suspension was sonicated 5  
142 min and stirred 2h at 60°C, and then the suspension was centrifuged, washed 3 times  
143 with 1:1 ethanol-distilled water solution, and the resulting precipitate was dried in an  
144 oven at 60°C for 48h.



145 **2.4 Preparation of oil-based drilling fluid**

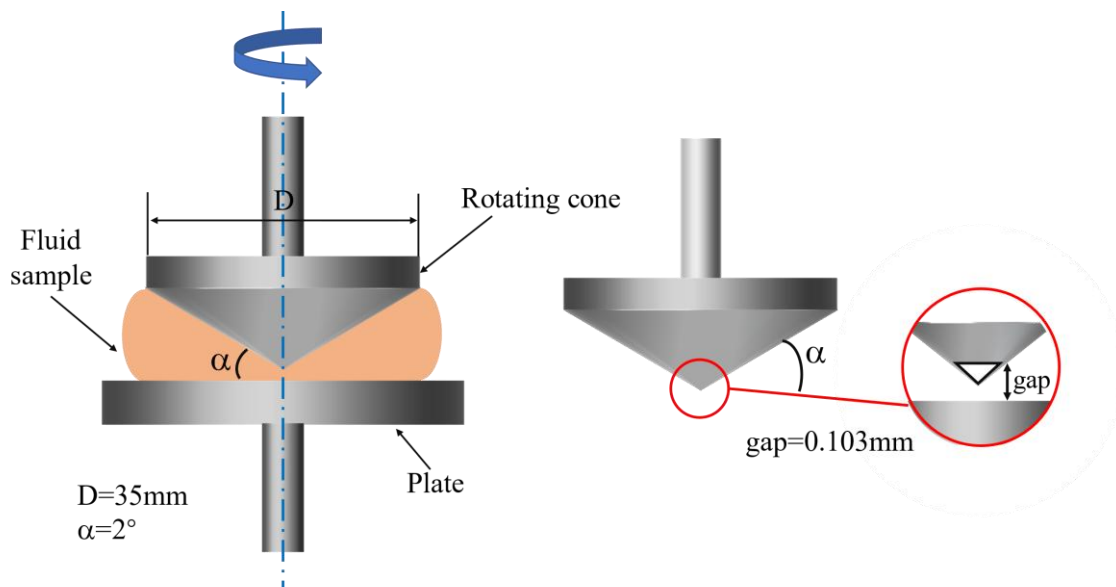
146 ZnOMt powder was added to paraffin oil and linseed oil, respectively, and stirred  
147 for 1h to prepare oil-based drilling fluid with a concentration of 50kg/m<sup>3</sup>. The drilling  
148 fluids should be aged at different temperatures to simulate the effect of formation  
149 temperature on drilling fluid properties during drilling operations. The resulting fluid  
150 was placed in a rotary oven heated to 60°C, 120°C, 180°C and kept for 16h. All the  
151 procedures follow the standards of American Petroleum Institute (API), i.e., API RP  
152 13D-2017 and API RP 13B-2-2018. The procedure for preparing ZnMt/oil drilling  
153 fluid and Zn/oil drilling fluid is the same as that for preparing ZnOMt/oil drilling fluid.  
154 The oil-based fluids were named following the template of ZnOMt/oil-temperature.  
155 For example, ZnOMt/paraffin-60 is prepared with ZnOMt and paraffin oil aged at  
156 60°C.

157 **2.5 Characterization**

158 The X-ray diffraction (XRD) patterns of all samples were conducted using  
159 Cu-K $\alpha$  radiation ( $\lambda=0.15406$  nm) on a Bruker D8 Advance X-ray powder  
160 diffractometer, which was performed at 40 kV, 30 mA and a scanning step of 0.05°. In  
161 particular, the XRD test procedure for ZnOMt/oil structure is described in detail in  
162 Section 3.1. The small drop of drilling fluid was placed on copper grids covered with  
163 an ultrathin carbon membrane for TEM analysis. The experiment was carried out with  
164 a JEOL 1011 transmission electron microscope, operating at the accelerating voltage  
165 of 100 kV (beam current around 86  $\mu$ A). The samples were imaged in Bright Field  
166 (BF) mode and were examined in high vacuum mode. Optical microscopy was carried

167 out by using an Olympus BX51 microscope to obtain the dispersion of ZnOMt in oil.

168 Rheology measurements were performed with a Thermo Fisher Scientific  
169 HAAKE MARS 40 rheometer, equipped with stainless steel cone plate fixtures to  
170 obtain a uniform flow field. Each measurement was repeated at least twice to check  
171 reproducibility. The geometry and parameters of the cone plate are shown in Fig. 1.  
172 The flow curves were measured in controlled shear rate mode, with the shear rate  
173 increasing linearly from  $0.1\text{s}^{-1}$  to  $1000\text{s}^{-1}$  in 180s. The thixotropy measurement  
174 process for oil-based drilling fluid was performed according to the following  
175 procedure: the shear rate linearly increased from  $0.1\text{s}^{-1}$  to  $1000\text{s}^{-1}$  in 180s (up-sweep),  
176 and then linearly decreased from  $1000\text{s}^{-1}$  to  $0.1\text{s}^{-1}$  in 180s (down-sweep). The  
177 calculation of the thixotropic loop area is performed using RheoWin 4.87. The  
178 dynamic viscoelastic properties of the samples were collected by oscillatory rheology  
179 tests. The strain amplitude sweep test from 0.1 to 100% strain was carried out at  
180  $\omega=6.28\text{ rad/s}$  to evaluate the linear viscoelastic range (LVER).



181

182

Fig. 1 The geometry and parameters of the cone plate fixture

## 183 **2.6 Rheological Modeling**

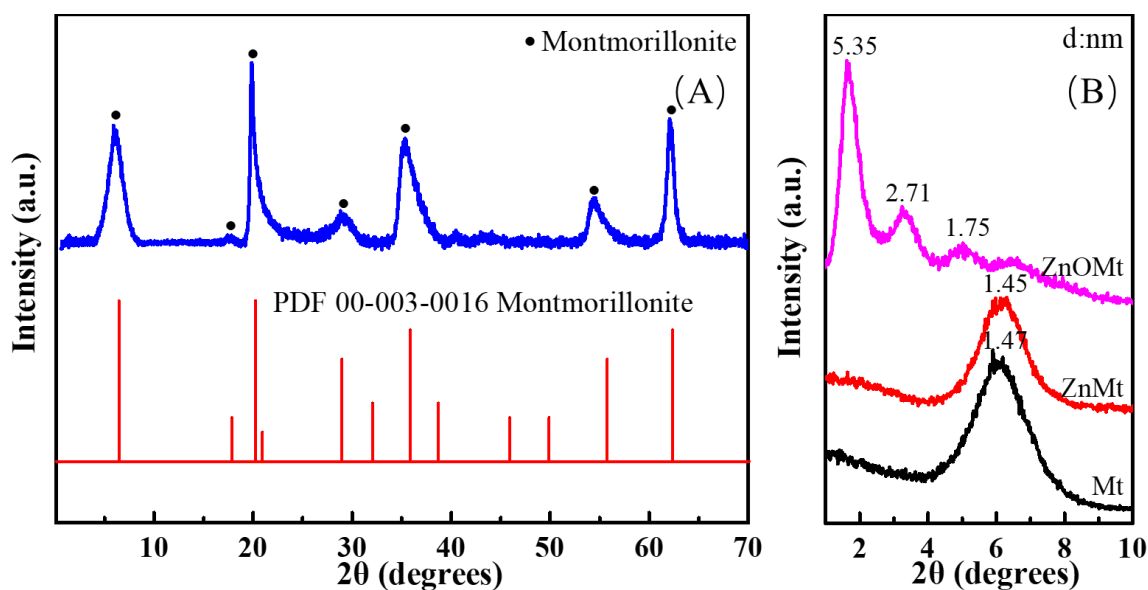
184 Rheological modeling aims to describe the flow behavior of drilling fluids  
185 mathematically. The rheological modeling for drilling fluid can facilitate the  
186 calculation of fluid flow dynamics (Agwu et al., 2021). Rheological models can  
187 generally be divided into two groups: (i) the relationship between shear rate and shear  
188 stress; (ii) the relationship between shear rate or shear stress and viscosity. In this  
189 study, the rheological data of the drilling fluid at different temperatures were fitted  
190 with three rheological models, including two-parameter models (i.e., Bingham-plastic,  
191 Casson) and three-parameter models (i.e., Herschel-Bulkey). More details and  
192 description of the rheological modeling are provided in the Supporting Information.

## 193 **3. Results and Discussion**

### 194 **3.1 X-ray diffraction**

195 The XRD patterns of the synthesized Mt and ZnOMt obtained by lecithin  
196 modification are presented in Fig. 2. The XRD pattern of synthesized Mt (Fig. 2A)  
197 matched well with the standard PDF card of Mt and no other reflections are observed,  
198 suggesting that Mt has been successfully synthesized and has a high purity. The Mt  
199 exhibited a reflection at  $2\theta=6.02^\circ$  with a  $d_{001}$ -value of 1.47nm. The XRD pattern of  
200 the ZnMt indicated little change in the intensity and position of the (001) reflection,  
201 which is consistent with the results of previous studies (Daković et al., 2012). After  
202 modification with lecithin, this reflection shifted to  $2\theta=1.65^\circ$ , corresponding to a basal  
203 spacing of 5.35nm. The basal spacing of ZnOMt increased from 1.45nm to 5.35nm  
204 (Fig. 2B), indicating the successful intercalation of lecithin into the interlayer space of

205 Mt.



206

207

Fig. 2 XRD patterns of synthesized Mt, ZnMt and ZnOMt

208

The structure of ZnOMt in oil is characterized by the XRD technique using a

209

suitable method (Fig. 3A). Firstly, a high-speed centrifuge was used to remove excess

210

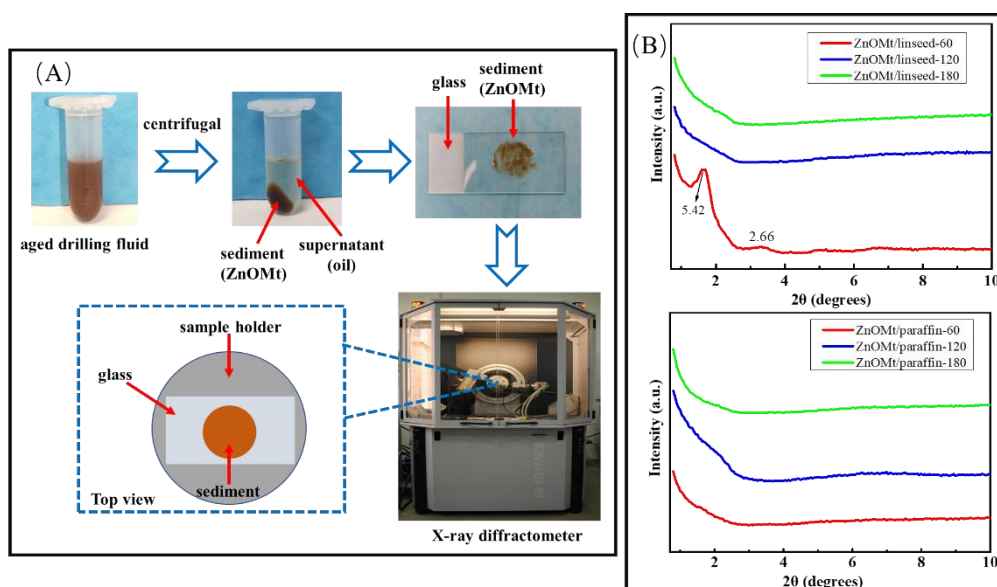
oil from the aged drilling fluid to obtain ZnOMt sediment. The ZnOMt sediment was

211

then uniformly smeared on the glass. Finally, the ZnOMt sediment can be measured

212

using the X-ray diffractometer, similar to powder samples.



213

214

Fig. 3 Interpretation diagram (A) of XRD test for ZnOMt sediment, and XRD patterns

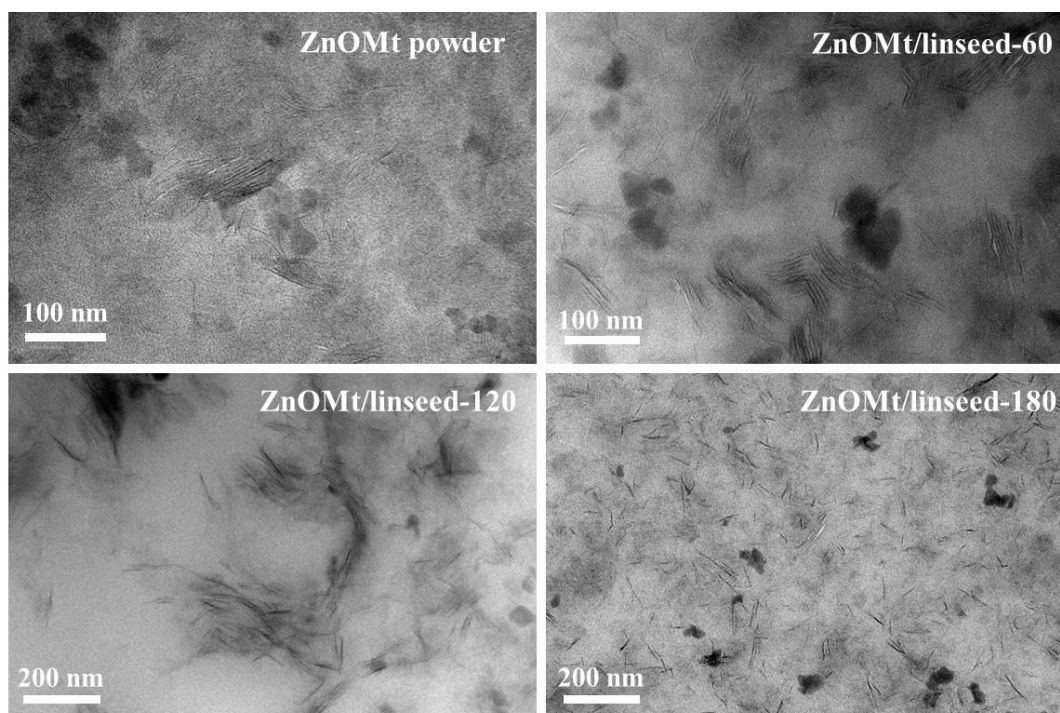
215 (B) of ZnOMt/linseed, ZnOMt/paraffin aged at different temperatures

216 The XRD patterns of ZnOMt sediment in linseed and paraffin oil aged at  
217 different temperatures are presented in Fig. 3B. The base spacing of the synthesized  
218 ZnOMt powder was 5.35 nm. However, the XRD results of ZnOMt/linseed and  
219 ZnOMt/paraffin showed different trends after aging at various temperatures. The basal  
220 spacing of ZnOMt/linseed-60 increased from 5.35 nm to 5.42 nm, suggesting the  
221 penetration of oil molecules into the interlayer of ZnOMt and subsequent expansion  
222 of the basal spacing. Based on previous research (Zhuang et al., 2017; Patel et al.,  
223 2019a), high temperatures can promote the thermal motion of oil molecules, leading  
224 to the swelling of ZnOMt in oil. There was no detectable reflection from Mt lattices in  
225 the XRD patterns of ZnOMt/linseed aged at 120°C and 180°C. The same results can  
226 also be observed in ZnOMt/paraffin systems. Several scholars suggested that the  
227 disappearance of the (001) reflection is caused by the exfoliation of organoclays in oil  
228 (Luckham and Rossi, 1999; Zhuang et al., 2016a; Zhuang et al., 2017). As the  
229 temperature increased, more oil molecules intercalated into the interlayer space of the  
230 ZnOMt, resulting in the exfoliation of clay platelets and reducing the attractive force  
231 between Mt sheets. The exfoliated clay platelets form a “house of cards” structure  
232 through three different modes of particle association : face-to-face (FF), edge-to-face  
233 (EF) and edge-to-edge (EE) (van Olphen, 1964). Others believed, however, that the  
234 qualitative structural information on d-spacing provided by XRD can not explain the  
235 different rheological properties observed in ZnOMt/oil systems, indicating that the  
236 basal spacing can not predict the fluid flow behavior (Burgentzlé et al., 2004;

237 Hermoso et al., 2014).

### 238 **3.2 TEM analysis**

239 In order to illustrate the microstructure of ZnOMt in oil-based drilling fluid,  
240 taking the ZnOMt/linseed system as an example, the TEM images of drilling fluid at  
241 different temperatures are shown in Fig. 4. The ZnOMt powder sample obtained by  
242 lecithin modification exhibited a layered structure. When it was dispersed in linseed  
243 oil and subjected to aging at 60°C, the layered structure remained unaltered, which is  
244 consistent with the XRD results. A large number of aggregated layered ZnOMt  
245 particles dispersed in the linseed oil. As the temperature increased to 120°C, the  
246 ZnOMt platelets exfoliated. The exfoliated nanoclay platelets were not randomly  
247 dispersed in the oil but formed compact clay tactoids and then a kind of network  
248 structure was formed. The ZnOMt/linseed-180 sample was completely exfoliated but  
249 presented a different dispersion state from ZnOMt/linseed-120. The ZnOMt platelets,  
250 of approximately 60 nm, were homogeneously dispersed in the linseed oil, without  
251 contact with each other. The network structure formed by the clay platelets was  
252 destroyed, because of the degradation of the surfactant in the ZnOMt at high  
253 temperature. The effect of temperature on the microstructure of ZnOMt is mainly  
254 reflected in the exfoliation and the degradation of surfactants. The relationship  
255 between the microstructure and rheological properties of ZnOMt in oil will be  
256 explained in detail in the following sections.



257

258 Fig. 4 TEM images of ZnOMt powder, and ZnOMt/linseed aged at different

259

temperatures

### 260 3.3 Dispersion

261

The dispersion states of ZnOMt and ZnMt powder in paraffin oil and linseed oil

262

at different temperatures were obtained mainly by optical microscopy for observing

263

the overall size distribution of the particles. As shown in Fig. 5, the ZnMt samples

264

were not uniformly dispersed throughout the organic medium for either paraffin oil or

265

linseed oil. Due to the strong hydrophilicity of ZnMt, it is difficult for oil molecules to

266

penetrate into the interlayer space to swell the clay particles. However, it is worth

267

noting that the dispersion of ZnMt in paraffin and linseed oil is distinct. The ZnMt

268

samples were randomly dispersed in linseed oil without any contact, whereas in

269

paraffin oil they were interconnected. These particles tend to gather and partially

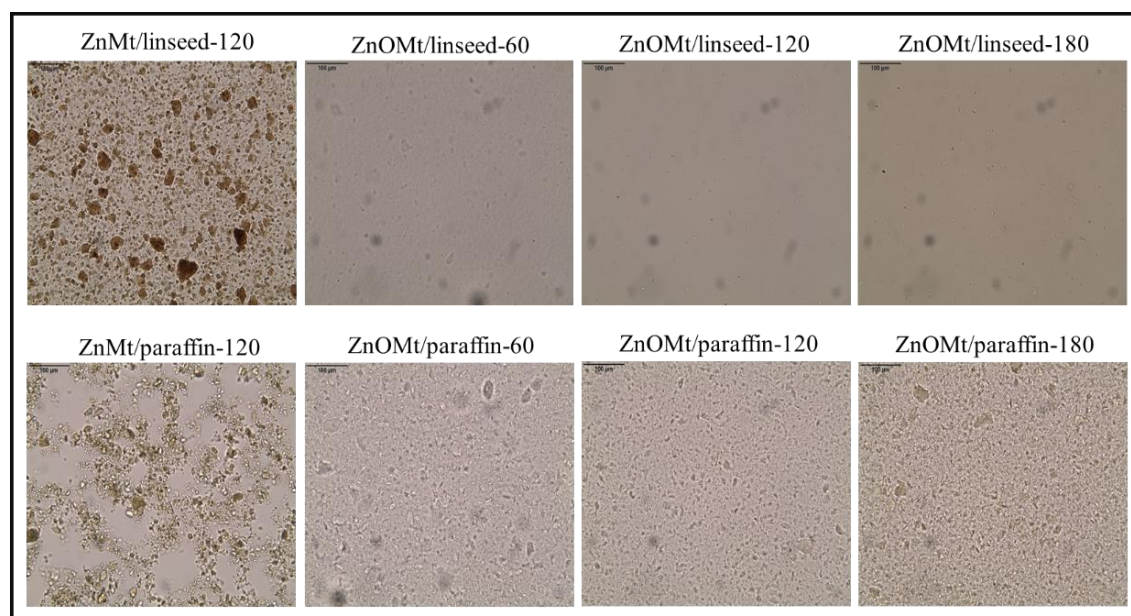
270

overlap each other and form a net-like structure. The organo-modification of ZnMt

271

with lecithin evidently improved its dispersion in oil. Although the dispersion of

272 ZnOMt in both oils was stable, the dispersion of ZnOMt in linseed oil was more  
273 homogeneous and the particle size was smaller. The ZnOMt in paraffin oil presented a  
274 large number of aggregated particles. In contrast, the aggregated particles in linseed  
275 oil were very limited at any temperature. This is probably due to the fact that linseed  
276 oil is polar compared to non-polar paraffin oil, which has a stronger affinity for  
277 ZnOMt modified by polar molecules of lecithin (Jones, 1983; Ma et al., 2023). In  
278 addition, temperature contributes to the dispersion of ZnOMt in oil-based drilling  
279 fluids.



280

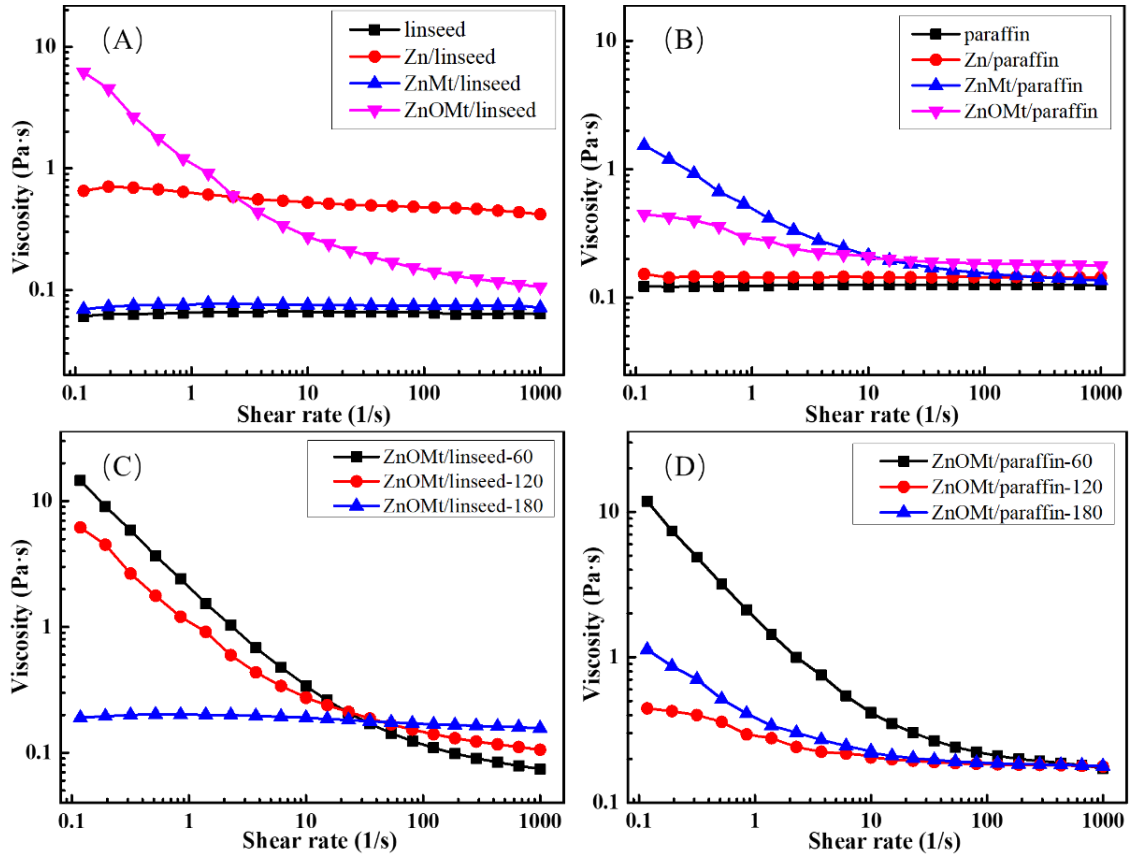
281 Fig. 5 Optical microscope images of ZnMt and ZnOMt in oil-based drilling fluid

### 282 **3.4 Rheological properties**

283 The relationship between shear stress and shear rate is the most accurate  
284 description of drilling fluid flow behavior (Arain et al., 2022). Fig. 6(A, B) illustrates  
285 the flow behavior of oil-based drilling fluid containing  $Zn^{2+}$ , ZnMt, ZnOMt samples  
286 as a function of shear rate at 120°C: different rheological behaviors were obtained in  
287 oil phases. Pure linseed and paraffin oil are Newtonian fluids, exhibiting a constant



288 viscosity at any shear rate. For linseed oil, the addition of  $Zn^{2+}$  remarkably increased  
289 the viscosity of linseed oil, and the viscosity of the system grew from 0.06 to 0.5 Pa·s,  
290 which may be caused by the saponification reaction between the zinc cations and the  
291 esters of the siccativ oil, as commonly reported in the literature (Osmond, 2019;  
292 Artesani, 2020). The addition of ZnMt had no effect on the viscosity of linseed oil,  
293 while ZnOMt modified its rheological behavior from Newtonian to shear thinning: the  
294 ZnOMt/linseed oil system displayed high viscosity at low shear rates and the viscosity  
295 decreased with increasing shear rates, which is highly desirable in drilling operations.  
296 For paraffin oil,  $Zn^{2+}$  did not affect the flow behavior of paraffin oil, as it is mainly  
297 composed of alkanes that cannot react with  $Zn^{2+}$ . Interestingly, paraffin oil containing  
298 ZnMt was a non-Newtonian fluid with shear thinning properties, while linseed oil  
299 containing ZnMt was a Newtonian fluid. This may be due to the different dispersion  
300 states of ZnMt in two oils. The net-like structure (Fig. 5) formed by ZnMt in paraffin  
301 oil leads to an increase in viscosity. Conversely, the dispersion of ZnOMt in paraffin  
302 oil did not yield satisfactory rheological properties. The ZnOMt showed better  
303 rheological performance and application potential for drilling fluid in linseed oil  
304 compared to paraffin oil.



305

306 Fig. 6 Flow tests of oil-based drilling fluids prepared by  $Zn^{2+}$ , ZnMt, ZnOMt at 120°C

307 (A, B) and flow tests of ZnOMt/oil fluids at varying temperatures (C, D)

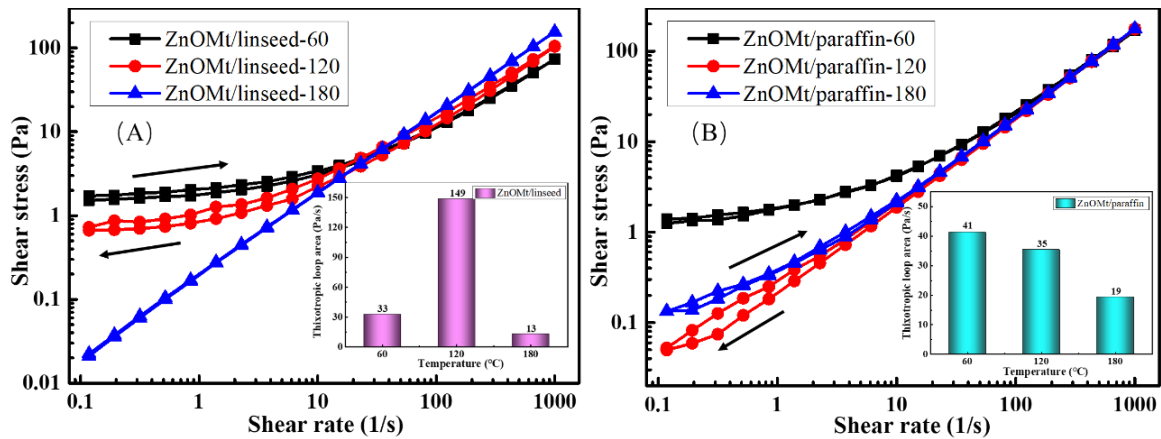
308 The rheological behavior of oil-based drilling fluid is not only affected by the oil  
 309 nature, but also depends on the temperature. As shown in Fig. 6(C, D), the rheological  
 310 properties of oil-based drilling fluids were altered as the temperature increased. At  
 311 temperatures below 120°C, ZnOMt/linseed fluids exhibited shear thinning behavior at  
 312 low shear rates. The viscosity measured at zero shear rate can be used to indicate the  
 313 pumpability of drilling fluids and as a rheological parameter to evaluate barite sag,  
 314 borehole cleaning, surge, and swab pressures (Maxey et al., 2008; Li et al., 2022). The  
 315 viscosity of ZnOMt/linseed oil systems at low shear rates decreased gradually with  
 316 increasing temperature. As the temperature increased to 180°C, the system viscosity  
 317 decreased to 0.2 Pa·s and became a Newtonian fluid. This reduction may be due to the

318 fact that temperature (180°C) disrupts the structure of clay platelets and reduces the  
319 connection and bonding between clay particles. The ZnOMt lost its ability to adjust  
320 linseed oil-drilling fluid rheological properties at 180°C, indicating that the  
321 electrochemical attraction between clay particles has totally disappeared. The  
322 ZnOMt/paraffin oil system exhibited similar rheological behavior to the  
323 ZnOMt/linseed oil fluid at 60°C. However, when the temperature rose to 120°C, its  
324 viscosity dropped significantly and tended to exhibit the properties of Newtonian fluid.  
325 Comparing the rheological properties of ZnOMt in linseed oil and paraffin oil, it can  
326 be concluded that the ZnOMt/linseed oil system is more resistant to high  
327 temperatures.

### 328 ***3.5 Thixotropy***

329 The thixotropy of the drilling fluid plays a crucial role in controlling the rate of  
330 penetration at low shear rates within the well annulus and ensuring effective  
331 suspension of cuttings (Celino et al., 2022). The microstructure of drilling fluid is  
332 disrupted in the up-sweep, while rebuilt in the down-sweep and hysteresis is induced  
333 in the flow curves. Fig. 7 illustrates the thixotropic loop curves of the ZnOMt/oil  
334 system at different temperatures. The loop areas of ZnOMt/linseed-60 and  
335 ZnOMt/linseed-180 fluids were minimal due to the lack of ZnOMt exfoliation at 60°C  
336 and the degradation of surfactant molecules at 180°C, resulting in poor thixotropy.  
337 Conversely, the loop area is higher at 120°C indicating greater thixotropy. According  
338 to XRD and TEM results, this is due to the exfoliation of ZnOMt and the resulting  
339 network structure in linseed oil. Based on the loop area values, the thixotropic loop

340 areas of the ZnOMt/paraffin system were not satisfactory, whatever the temperature.



341

342 Fig. 7 The thixotropic loop curves and areas of the ZnOMt/linseed (A) and

343 ZnOMt/paraffin (B) system at different temperatures

### 344 3.6 Rheological modeling

345 The knowledge of the drilling fluid rheological model is crucial, as the accuracy  
346 of fitting the model to the actual properties of the drilling fluid will dramatically affect  
347 the drilling hydraulics calculations (Wiśniowski et al., 2020). In this work, the  $R^2$ ,  
348 SSR, and RMSE are used to determine the performance of the rheological models.  
349 These parameters were defined by fitting constants using regression analysis obtained  
350 from rheological data. The curve fitting of the rheology model at different  
351 temperatures, including the obtained rheological constants and derived statistical  
352 parameters, is provided in the Supporting Information.

353 A satisfactory model to characterize the rheological properties of drilling fluids at  
354 different temperatures was determined based on the values of fitted parameters such  
355 as  $R^2$  (greater than 0.99), SSR (less than 5) and RMSE (less than 0.2) (Rafieefar et al.,  
356 2021). As expected, the Bingham-plastic model was not suitable for describing the  
357 rheological behavior of non-Newtonian drilling fluid because the model expresses a

358 linear relationship. In comparison with the Bingham-plastic model, the Casson model  
359 fitted better, revealing the nonlinear relationship between the shear stress and shear  
360 rate. The Herschel-Bulkey model represents the most accurate fitting results of  
361 drilling fluids at different temperatures. This is why the Herschel-Bulkley model is  
362 selected for utilization in the drilling fluid field.

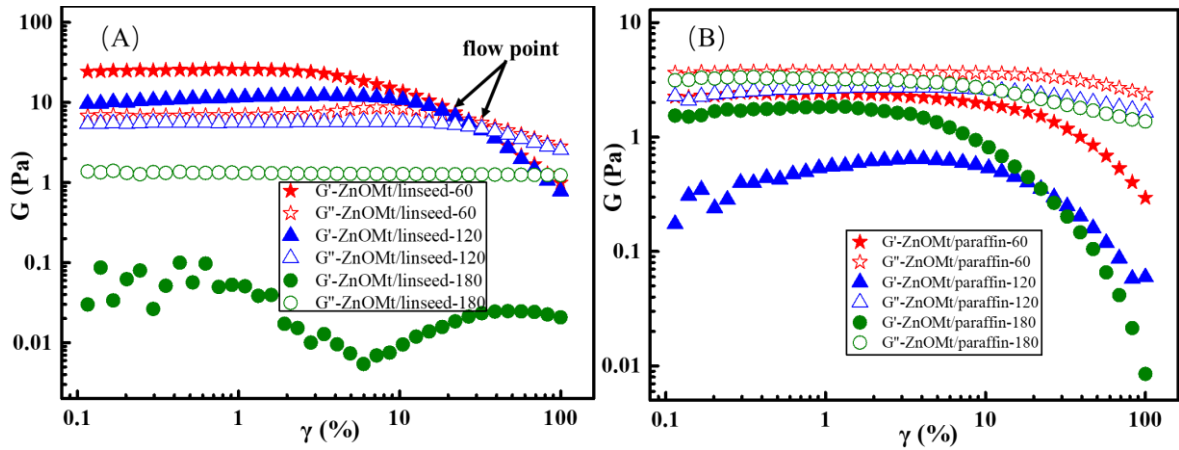
363 Rheological parameters such as flow behavior index ( $n$ ) and consistency  
364 coefficient ( $k$ ) obtained by the Herschel-Bulkley model provide more valuable  
365 information. The  $n$  value can be used to evaluate the ability of drilling fluids to carry  
366 cuttings, and  $k$  is the measure of the consistency of the fluid, which is proportional to  
367 the effective viscosity (Maiti et al., 2021). The drilling fluid with the lowest  $n$  value  
368 and the highest  $k$  value has a greater ability to suspend and carry drill cuttings. The  
369 fitting results obtained from the Herschel-Bulkley model revealed that the  
370 ZnOMt/linseed system exhibited an  $n$  value of 0.8884 and a  $k$  value of 0.2263 at  
371 120°C. These findings indicate that the linseed oil-based drilling fluid demonstrated  
372 the most favorable rheological properties at 120°C.

### 373 ***3.7 Viscoelastic properties***

374 Dynamic measurements were also performed on ZnOMt/oil systems to  
375 understand their structural behavior (Werner et al., 2017). The amplitude sweep tests  
376 are presented in Fig. 8, indicating the viscoelastic properties (storage and loss  
377 modulus) of the ZnOMt/oil system at different temperatures.

378 The linear viscoelastic range (LVER) is defined by the strain range where  $G'$  and  
379  $G''$  are approximately constant: the limit of the LVER was 3% for ZnOMt/linseed-60

380 and 8% for ZnOMt/linseed-120, respectively. The microstructure of the drilling fluid  
381 within the LVER remains intact; it is a solid-like structure as the value of  $G'$  was  
382 higher than that of  $G''$ . When the drilling fluid is subjected to greater strain after the  
383 LVER, micro-cracks begin to appear, which spread throughout the drilling fluid  
384 system and this behavior persists until the flow point is achieved (Medhi et al., 2021).  
385 The flow point ( $G'=G''$ ) represents the overlapping point of  $G'$  and  $G''$ , implying a  
386 transition from solid-like to liquid-like characteristics. As the strain increased after the  
387 flow point,  $G'<G''$  and the drilling fluid behaved more like a liquid-like and viscous  
388 structure. With increasing temperature, the flow point shifted towards higher shear  
389 strain. The flow points corresponding to ZnOMt/linseed-60 and ZnOMt/linseed-120  
390 were 25% and 34%, respectively. Higher flow point normally related to stronger inner  
391 structure and suspension capacity. At 180°C,  $G'' > G'$  regardless of the applied strain,  
392 indicating liquid-like behavior: the internal structure of the sample was completely  
393 disrupted, which is consistent with the TEM results. The ZnOMt/paraffin systems did  
394 not exhibit any viscoelasticity with  $G''$  always greater than  $G'$  at both high and low  
395 temperatures. This result suggested that ZnOMt prepared from lecithin could not  
396 form a network structure in paraffin oil. The composition and nature of the base oil is  
397 also an important factor in the viscoelasticity of the drilling fluid.



398

399 Fig. 8 The amplitude sweep tests of the ZnOMt/linseed (A) and ZnOMt/paraffin (B)

400

systems at different temperatures

### 401 3.8 Discussion of rheological mechanism

402

Based on the experimental findings, a comprehensive analysis of the impact of

403

temperature on the rheological properties of linseed oil-based drilling fluid and the

404

microstructure of ZnOMt in linseed oil is thoroughly discussed. A schematic

405

representation of the microstructure of ZnOMt in linseed oil at different temperatures

406

is proposed in Fig. 9. The synthesized ZnOMt maintained the layered structure while

407

exhibiting an increased interlayer spacing, suggesting the intercalation of lecithin.

408

This observation is further supported by the XRD and TEM results. After the

409

dispersion of ZnOMt in linseed oil at 60°C, no exfoliation has been observed. The

410

aggregation of larger clay particles impeded the flow of drilling fluid and resulted in

411

higher viscosity. In addition, the high aspect ratio of the ZnOMt further reinforced this

412

flow resistance (Cruz et al., 2019). When the temperature rose to 120°C, the oil

413

molecules intercalated into the interlayer space and caused exfoliation of the ZnOMt

414

(van Olphen, 1964; Luckham and Rossi, 1999). Lecithin molecules adsorbed on the

415

surface of ZnOMt possess long and flexible alkyl chains, which facilitated their

416 entanglement with each other, leading to a physical attraction (Zhuang et al., 2016b;  
417 Liu et al., 2023). By increasing the temperature up to 180°C, lecithin molecules started  
418 to degrade, and the network structure of the drilling fluid was completely destroyed.  
419 The exfoliation of ZnOMt leading to its homogeneous dispersion in oil was confirmed  
420 by observations using optical microscopy and TEM.

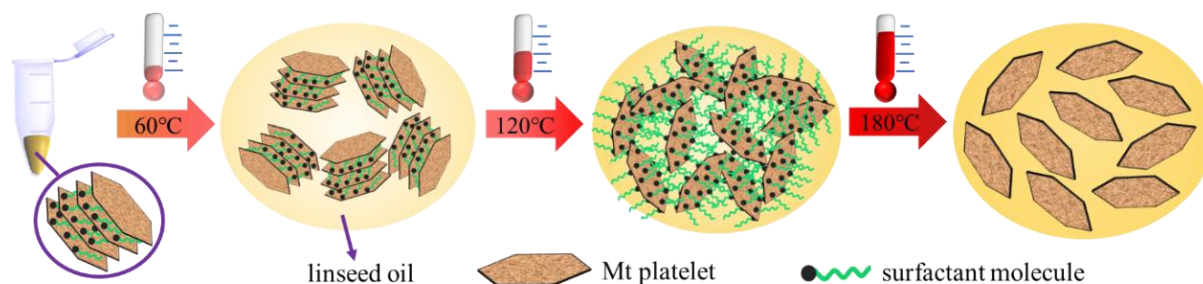


Fig. 9 The microstructure of ZnOMt in linseed oil at different temperatures

#### 423 **4. Conclusions**

424 A systematic and in-depth experimental work was performed to probe the  
425 potential of siccative oil (linseed oil) as an alternative to mineral oil-based drilling  
426 fluid. The viscoelasticity, thixotropy, and microstructure of ZnOMt in linseed oil and  
427 paraffin oil at different temperatures were compared and investigated. The ZnOMt  
428 prepared by zinc ions and lecithin showed viscoelastic behavior in linseed oil when  
429 the temperature didn't succeed 120 °C. The microstructure of ZnOMt in linseed oil  
430 undergoes three stages with rising temperature: swelling→exfoliation→high  
431 dispersion. The association of exfoliated clay platelets and the intertwining of  
432 surfactant molecules adsorbed on the clay surface are the basis for forming a network  
433 structure and thixotropy in drilling fluids. In addition, the paraffin oil-based drilling  
434 fluids always displayed liquid-like behavior, while linseed oil-based drilling fluids  
435 exhibited viscoelastic properties and maximum thixotropy at 120°C. The favorable



436 properties of vegetable oil-based drilling fluids containing organoclays provide great  
437 potential for their application in drilling engineering.

#### 438 *Acknowledgments*

439 Qiang Li is grateful for the scholarship (No. 202006440010) awarded by the  
440 China Scholarship Council (CSC). This project was funded by the Region Ile de  
441 France, DIM-MAP “Matériaux anciens et patrimoniaux” (project RheoPaint).

#### 442 *References*

443 Agwu, O.E., Akpabio, J.U., Ekpenyong, M.E., Inyang, U.G., Asuquo, D.E., Eyoh, I.J., Adeoye,  
444 O.S., 2021. A critical review of drilling mud rheological models. *Journal of Petroleum Science*  
445 *and Engineering* 203, 108659.

446 Agwu, O.E., Okon, A.N., Udoh, F.D., 2015. A comparative study of diesel oil and soybean oil  
447 as oil-based drilling mud. *Journal of Petroleum Engineering* 2015, 1-10.

448 Arain, A.H., Ridha, S., Mohyaldinn, M.E., Suppiah, R.R., 2022. Improving the performance of  
449 invert emulsion drilling fluid using boron nitride and graphene nanoplatelets for drilling of  
450 unconventional high-temperature shale formations. *Journal of Molecular Liquids* 363, 119806.

451 Aramendiz, J., Imqam, A., 2019. Water-based drilling fluid formulation using silica and  
452 graphene nanoparticles for unconventional shale applications. *Journal of Petroleum Science*  
453 *and Engineering* 179, 742-749.

454 Artesani, A., 2020. Zinc oxide instability in drying oil paint. *Materials Chemistry and Physics*  
455 255, 123640.

456 Burgentzié, D., Duchet, J., Gérard, J., Jupin, A., Fillon, B., 2004. Solvent-based  
457 nanocomposite coatings: I. Dispersion of organophilic montmorillonite in organic solvents.

458 Journal of colloid interface science 278, 26-39.

459 Celino, K.N., Fernandes, R.d.S., de Moraes, S.C., de Souza, E.A., Balaban, R.d.C., 2022.

460 Emulsion-based drilling fluids: Rheological properties preservation facing changes on the

461 temperature, pressure and dispersed phase. Journal of Molecular Liquids 352, 118753.

462 Cruz, N., Forster, J., Bobicki, E.R., 2019. Slurry rheology in mineral processing unit operations:

463 A critical review. The Canadian Journal of Chemical Engineering 97, 2102-2120.

464 Daković, A., Kragović, M., Rottinghaus, G.E., Ledoux, D.R., Butkeraitis, P., Vojislavljević, D.Z.,

465 Zarić, S.D., Stamenić, L., 2012. Preparation and characterization of zinc-exchanged

466 montmorillonite and its effectiveness as aflatoxin B1 adsorbent. Materials Chemistry and

467 Physics 137, 213-220.

468 de Brito Buriti, B.M.A., Barsosa, M.E., da Silva Buriti, J., de Melo Cartaxo, J., Ferreira, H.S., de

469 Araújo Neves, G., 2022. Modification of palygorskite with cationic and nonionic surfactants for

470 use in oil-based drilling fluids. Journal of Thermal Analysis and Calorimetry 147, 2935-2945.

471 de Oliveira, L.H., Trigueiro, P., Rigaud, B., da Silva-Filho, E.C., Osajima, J.A., Fonseca, M.G.,

472 Lambert, J.-F., Georgelin, T., Jaber, M., 2021. When RNA meets montmorillonite: Influence of

473 the pH and divalent cations. Applied Clay Science 214, 106234.

474 de Viguerie, L., Payard, P.A., Portero, E., Walter, P., Cotte, M., 2016. The drying of linseed oil

475 investigated by Fourier transform infrared spectroscopy: Historical recipes and influence of

476 lead compounds. Progress in Organic Coatings 93, 46-60.

477 Deville, J.P., Fritz, B., Jarrett, M., 2011. Development of Water-Based Drilling Fluids

478 Customized for Shale Reservoirs. SPE Drilling & Completion 26, 484-491.

479 Hermoso, J., Martinez-Boza, F., Gallegos, C., 2014. Influence of viscosity modifier nature and

480 concentration on the viscous flow behaviour of oil-based drilling fluids at high pressure.  
481 Applied Clay Science 87, 14-21.

482 Jaber, M., Miéhé-Brendlé, J., 2005. Influence du milieu de synthèse sur la cristallisation de  
483 saponite : proposition de mécanisme réactionnel en milieux acide et basique. Comptes  
484 Rendus Chimie 8, 229-234.

485 Jones, T.R., 1983. The properties and uses of clays which swell in organic solvents. Clay  
486 Minerals 18, 399-410.

487 Li, Q., Berraud-Pache, R., Souprayen, C., Jaber, M., 2023a. Intercalation of lecithin into  
488 bentonite: pH dependence and intercalation mechanism. Applied Clay Science 244, 107079.

489 Li, Q., Berraud-Pache, R., Yang, Y., Souprayen, C., Jaber, M., 2023b. Biocomposites based  
490 on bentonite and lecithin: An experimental approach supported by molecular dynamics.  
491 Applied Clay Science 231, 106751.

492 Li, X.-L., Jiang, G.-C., Xu, Y., Deng, Z.-Q., Wang, K., 2022. A new environmentally friendly  
493 water-based drilling fluids with laponite nanoparticles and polysaccharide/polypeptide  
494 derivatives. Petroleum Science 19, 2959-2968.

495 Liu, S., Zhang, C., Du, J., Huang, H., Fang, S., Li, X., Duan, M., 2023. Effect of dispersants on  
496 the stability of calcite in non-polar solutions. Colloids and Surfaces A: Physicochemical and  
497 Engineering Aspects 672, 131730.

498 Luckham, P.F., Rossi, S., 1999. The colloidal and rheological properties of bentonite  
499 suspensions. Advances in Colloid and Interface Science 82, 43-92.

500 Ma, G.-D., Zuo, H.-R., Pang, S.-Y., Duan, M., Xiong, Y., Li, X.-L., 2023. Anchoring polyamide  
501 active layer to improve the thermal stability of polyacrylonitrile composite forward osmosis

502 membrane through interfacial enthalpic effect. *Separation and Purification Technology* 318,  
503 123954.

504 Maiti, M., Bhaumik, A.K., Mandal, A., 2021. Performance of water-based drilling fluids for  
505 deepwater and hydrate reservoirs: Designing and modelling studies. *Petroleum Science* 18,  
506 1709-1728.

507 Malamis, S., Katsou, E., 2013. A review on zinc and nickel adsorption on natural and modified  
508 zeolite, bentonite and vermiculite: Examination of process parameters, kinetics and isotherms.  
509 *Journal of Hazardous Materials* 252-253, 428-461.

510 Maxey, J., Ewoldt, R., Winter, P., McKinley, G., 2008. Yield stress: what is the True value,  
511 *AADE Fluids Conference and Exhibition*, pp. 1-10.

512 Medhi, S., Gupta, D.K., Sangwai, J.S., 2021. Impact of zinc oxide nanoparticles on the  
513 rheological and fluid-loss properties, and the hydraulic performance of non-damaging drilling  
514 fluid. *Journal of Natural Gas Science and Engineering* 88, 103834.

515 Moraru, V.N., 2001. Structure formation of alkylammonium montmorillonites in organic media.  
516 *Applied Clay Science* 19, 11-26.

517 Orlova, Y., Harmon, R.E., Broadbelt, L.J., Iedema, P.D., 2021. Review of the kinetics and  
518 simulations of linseed oil autoxidation. *Progress in Organic Coatings* 151, 106041.

519 Osmond, G., 2019. Zinc soaps: an overview of zinc oxide reactivity and consequences of soap  
520 formation in oil-based paintings. *Metal soaps in art: Conservation research*, 25-46.

521 Patel, H.A., Santra, A., Thaemlitz, C.J., 2019a. Exceptional flat rheology using a synthetic  
522 organic-inorganic hybrid in oil-based muds under high pressure and high temperature,  
523 *SPE/IADC International Drilling Conference and Exhibition*. OnePetro.

524 Patel, H.A., Santra, A., Thaemlitz, C.J., 2019b. Exceptional Flat Rheology Using a Synthetic  
525 Organic-Inorganic Hybrid in Oil-Based Muds Under High Pressure and High Temperature,  
526 SPE/IADC International Drilling Conference and Exhibition, p. D012S020R001.

527 Pereira, L.B., Sad, C.M.S., Castro, E.V.R., Filgueiras, P.R., Lacerda, V., 2022. Environmental  
528 impacts related to drilling fluid waste and treatment methods: A critical review. Fuel 310,  
529 122301.

530 Rafieefar, A., Sharif, F., Hashemi, A., Bazargan, A.M., 2021. Rheological Behavior and  
531 Filtration of Water-Based Drilling Fluids Containing Graphene Oxide: Experimental  
532 Measurement, Mechanistic Understanding, and Modeling. ACS Omega 6, 29905-29920.

533 Sulaimon, A.A., Adeyemi, B.J., Rahimi, M., 2017. Performance enhancement of selected  
534 vegetable oil as base fluid for drilling HPHT formation. Journal of Petroleum Science and  
535 Engineering 152, 49-59.

536 van Olphen, H., 1964. Internal mutual flocculation in clay suspensions. Journal of Colloid  
537 Science 19, 313-322.

538 Werner, B., Myrseth, V., Saasen, A., 2017. Viscoelastic properties of drilling fluids and their  
539 influence on cuttings transport. Journal of Petroleum Science Engineering 156, 845-851.

540 Wiśniowski, R., Skrzypaszek, K., Małachowski, T., 2020. Selection of a Suitable Rheological  
541 Model for Drilling Fluid Using Applied Numerical Methods, Energies.

542 Yan, H., Zhang, Z., 2021. Effect and mechanism of cation species on the gel properties of  
543 montmorillonite. Colloids and Surfaces A: Physicochemical and Engineering Aspects 611,  
544 125824.

545 Zhong, H., Guan, Y., Qiu, Z., Grady, B.P., Su, J., Huang, W., 2023. Application of carbon

546 coated bentonite composite as an ultra-high temperature filtration reducer in water-based  
547 drilling fluid. *Journal of Molecular Liquids* 375, 121360.

548 Zhuang, G., Gao, J., Peng, S., Zhang, Z., 2019. Synergistically using layered and fibrous  
549 organoclays to enhance the rheological properties of oil-based drilling fluids. *Applied Clay*  
550 *Science* 172, 40-48.

551 Zhuang, G., Zhang, H., Wu, H., Zhang, Z., Liao, L., 2017. Influence of the surfactants' nature  
552 on the structure and rheology of organo-montmorillonite in oil-based drilling fluids. *Applied*  
553 *Clay Science* 135, 244-252.

554 Zhuang, G., Zhang, Z., Sun, J., Liao, L., 2016a. The structure and rheology of  
555 organo-montmorillonite in oil-based system aged under different temperatures. *Applied Clay*  
556 *Science* 124-125, 21-30.

557 Zhuang, G., Zhang, Z., Sun, J., Liao, L., 2016b. The structure and rheology of  
558 organo-montmorillonite in oil-based system aged under different temperatures. *Applied Clay*  
559 *Science* 124, 21-30.

560